Nanoindentation study of thin plasma enhanced chemical vapor deposition SiCOH low-*k* films modified in He/H_2 downstream plasma

Kris Vanstreels[a)]
Interuniversity MicroElectronics Centre (IMEC), Kapeldreef 75, B-3001 Leuven, Belgium

Adam M. Urbanowicz
Interuniversity MicroElectronics Centre (IMEC), Kapeldreef 75, B-3001 Leuven, Belgium and Department of Chemistry, Katholieke Universiteit Leuven, B-3001 Leuven, Belgium

(Received 27 May 2009; accepted 21 December 2009; published 20 January 2010)

The effect of He/H_2 downstream plasma (DSP) on the mechanical properties of plasma enhanced chemical vapor deposition SiCOH low-*k* films was studied using nanoindentation (NI) with the continuous-stiffness measurement technique. Furthermore, the main requirements for reliable NI measurements on plasma-modified low-*k* films are discussed. The results show that the mechanical properties of these films are intimately linked with their porosity and that exposure to He/H_2 DSP causes a change in both the porosity and the mechanical properties of the films. This change is related to the removal of porogen residue formed during the ultraviolet curing of the low-*k* film.
 [DOI: 10.1116/1.3293200]

I. INTRODUCTION

The integration of copper metal wiring and intermetal low-*k* materials has become crucial for next-generation integrated circuit interconnect technology with low interconnect resistive capacitive delay and allowing higher current densities. Recently, a number of low-*k* dielectric materials have been developed to replace SiO_2 as an intermetal dielectric in microelectronic devices.[1] These new materials must provide both the electrical advantages of a lower dielectric constant and a sufficient structural support for the embedded copper wires used in state-of-the-art damascene processing. This requires a good compatibility with modern semiconductor processes and, therefore, places stringent demands on their mechanical stability, in both manufacturing and reliability.[2–4] Recently used low-*k* materials in the Cu/low-*k* integration scheme have *k*-values between 2.5 and 3.0. One of the limiting factors in further reduction in *k*-value is mechanical robustness since more than 32% of porosity needs to be introduced into plasma enhanced chemical vapor deposition (PECVD) low-*k* films in order to achieve *k*-values be low 2.3.

SiCOH-type low-*k* materials contain a SiO_2-like matrix where part of the terminating oxygen atoms is replaced by organic groups (most often CH_3). Porosity in advanced SiCOH-type low-*k* films is created after deposition through the use of a sacrificial phase (porogen) that is removed by ultraviolet (UV)-assisted thermal curing. Porogen residue inside the PECVD low-*k* films is a nonvolatile product of UV photochemical dissociation of porogen. The amount of porogen residue after UV curing depends on the deposition conditions, porosity, and UV curing conditions.[5] Recently, it was found that the porogen residue in PECVD low-*k* films can be removed by He/H_2 plasma.[6,7] Figure 1 illustrates the absorption spectrum of UV-cured (solid lines) and 700 s He/H_2 plasma-modified (dashed line) low-*k* films. The absorption bands located between 200 and 300 nm are related to the presence of amorphous carbonlike porogen residue.[8,9] Plasma exposure completely removed the porogen residue from the low-*k* film and the final absorption spectrum is similar to UV spectra of low-*k* matrix material. Porogen removal results in an increased film porosity, which reduces inter-related properties responsible for the mechanical stability of low-*k* materials: Young's modulus, hardness, fracture toughness, and interfacial adhesion. The latter phenomenon is related to He/H_2 plasma effect and might be a new challenge for Cu/low-*k* integration of advanced PECVD low-*k* materials.[7] The He/H_2 downstream plasma is the most attractive option for photoresist mask removal due to the minimal effect on the degradation of the dielectric constant of low-*k* film during the ash process.[6,10,11] Therefore, it is necessary to perform a detailed study of mechanical properties of low-*k* film upon He/H_2 plasma exposure.

This article focuses on the He/H_2 plasma effect on the mechanical properties of four different PECVD low-*k* films using nanoindentation (NI) and the main requirements for reliable NI measurement of these plasma-modified low-*k* films. NI is a powerful technique for measuring mechanical properties of thin films, including low-*k* dielectric materials.[12–18] However, accurate characterization of the mechanical properties of soft porous thin films has significant limitations. One of the major concerns in using nanoindentation on thin soft films is related to the spatial extent of the elastic-deformation field in the film, which extends well beyond the actual depth of indentation and can result in an overestimation of the true Young's modulus of the film.[14,19,20,15,21,22] The value of Young's modulus is very often used as an indicator of the mechanical stability of low-*k* dielectric materials.[18] Therefore, shallow indentation depths are needed and a great deal of care needs to be taken with

a)Author to whom correspondence should be addressed; electronic mail: kris.vanstreels@imec.be

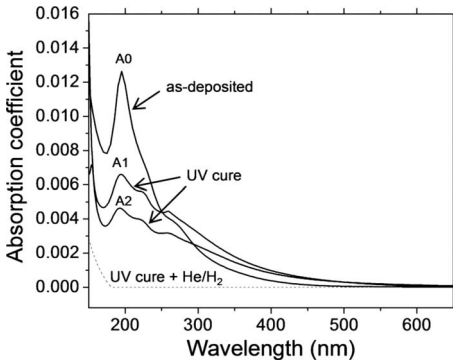

FIG. 1. Absorption spectrum of an as-deposited, UV-cured (solid lines), and 700s He/H_2 plasma-modified (dashed line) low-*k* films as measured by UV-SE.

regard to the tip shape calibration, surface contact determination, relaxation phenomena, and film porosity effects in order to get reliable data.[19]

This work contains two parts. The first part (A) is devoted to key factors influencing reliability of NI study of thin low-*k* films. The second part (B) focuses on the He/H_2 downstream plasma (DSP) plasma effect (i.e., porogen residue removal) on the mechanical properties of SiCOH low-*k* films using the NI technique.

II. EXPERIMENTAL DETAILS

Porous SiCOH-type low-*k* dielectric films of 180 nm with porosity in the range of 13%–34% were deposited on 300 mm silicon wafers using a PECVD porogen-based process and then afterward, treated with He/H_2 DSP using different exposure times. The matrix material was codeposited with sacrificial porogen by PECVD and subsequently, UV cured in nitrogen ambient at temperatures close to 430 °C. These films were all deposited in exactly the same condition, but were cured using two different UV sources (Table I). The *k*-values of the UV-cured films were in the range of 2.3. The He/H_2 20:1 DSP treatments of blanket low-*k* films were performed in a downstream plasma stripper. The films were treated with He/H_2 DSP at a fixed substrate temperature of 280 °C using varied times in the range of 20–700 s. The open porosity and pore size distributions were evaluated using ellipsometric porosimetry. Young's modulus and hardness of the low-*k* dielectric films were measured by the nanoindentation technique using a nanoindenter XP system (MTS Systems Corporation) with a dynamic contact module and a continuous-stiffness measurement (CSM) option under constant strain rate condition (0.05 s^{-1}). A standard three-sided pyramid diamond indenter tip (Berkovich) was used for the indentation experiments. As the indenter tip was pressed into each sample, both depth of penetration (h) and the applied load (P) were monitored. Next, a load-versus-depth curve was generated from the collected data. At the maximum indentation depth, the load was kept constant for 10 s. No significant creep was observed in all samples. During the subsequent unloading segment, the tip is withdrawn to 10% of the maximum load and then held in contact with the surface for 60 s. The latter was used to correct the thermal drift. From the experimentally obtained load-displacement curve, Young's modulus (E) and hardness (H) can be calculated based on their relationship with the contact area and the measured contact stiffness (S),

$$S = \beta \frac{2}{\sqrt{\pi}} E_r \sqrt{A}, \tag{1}$$

$$H = \frac{P_{\max}}{A}, \tag{2}$$

where A is the projected contact area of the indenter with the sample surface and E_r is the effective Young's modulus defined by

$$E_r = \left[\frac{1-\nu^2}{E} + \frac{1-\nu_i^2}{E_i} \right]^{-1}. \tag{3}$$

The effective Young's modulus takes into account the fact that elastic displacements occurred in both the sample, with Young's modulus E and Poisson's ratio ν, and the indenter with elastic constants E_i (1140 GPa) and ν_i (0.07). Since Poisson's ratio is not well known for SiCOH low-*k* films, it was varied between 0.17 and 0.3 during data analysis. The contact area (A) was determined from the indenter tip shape calibration. The contact stiffness was determined during the loading segments of the indentation tests using the CSM technique. This was accomplished by superimposing an alternating force with known frequency, amplitude, and phase on the nominal applied force. This oscillating force then resulted in a displacement oscillation, $h(\omega) = h_0 \exp(i\omega t + \phi)$, where ω is the applied oscillation frequency, h_0 is the amplitude, and ϕ is the phase angle between the force and displacement signals. The displacement response of the indenter at the excitation frequency (~75 Hz) and the phase angle between the force and displacement were then measured continuously as a function of the indentation depth. The phase

TABLE I. Summary of physical properties of as-deposited and UV-cured SiCOH low-*k* materials.

Film	Thickness (nm)	Total film porosity (%)	Mean pore radii (nm)	*k*-value	Young's modulus (GPa)	Hardness (GPa)	Curing UV source wavelength (nm)
A0	180	13	0.5	3.0	6.3 ± 0.6	0.53 ± 0.03	No UV curing
A1	180	32	0.9	2.3	4.5 ± 0.2	0.39 ± 0.03	~172 (narrow band)
A2	180	34	1.0	2.3	3.8 ± 0.3	0.36 ± 0.04	>200 (broad band)

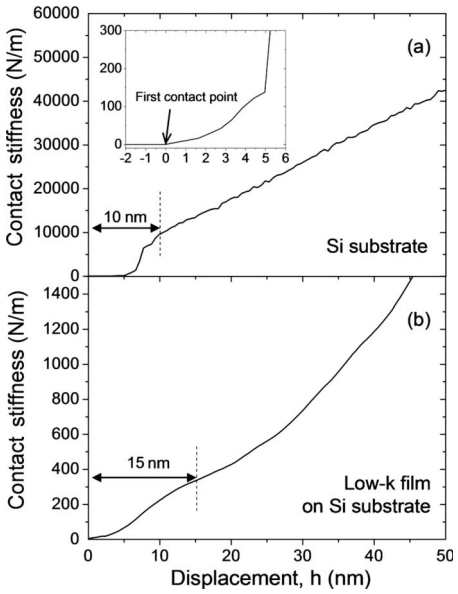

FIG. 2. Contact-stiffness measurements as a function of indentation depth for (a) silicon substrate; (b) SiCOH-like low-*k* film on a silicon substrate.

and amplitude of this response are characteristic of the materials' properties. To investigate the deformation of the films during a complete indentation cycle, several indents at different depths were made and observed with a scanning electron microscopy (SEM).

III. RESULTS AND DISCUSSION

A. Key factors influencing reliability of NI study of thin low-*k* films

Before showing the impact of He/H_2 DSP plasma on the mechanical properties of SiCOH low-*k* films, we first draw attention to several challenges that are encountered during data analysis, but are very often easily overseen. Obtaining accurate reliable data on thin soft films requires (1) an accurate surface contact determination, (2) a reduced spatial extent of the elastic-deformation field, (3) a calibration that is accurate enough at very low indentation depths, and (4) the determination of a critical penetration depth for coating-only properties. This sets stringent demands on the nanoindentation equipment and on the quality of the indenter tip. All these aspects will be discussed in Secs. III A 1–III A 4.

1. Surface-contact determination

During indentation experiments, the displacement is ideally measured from the level of the specimen-free surface. In practice, the indenter must first make contact with the specimen before the displacements can be taken. The depth at which this happens is then taken as a reference point for all further indentation depths. Figure 2 shows the contact stiffness before [Fig. 2(a)] and after [Fig. 2(b)] deposition of a low-*k* film on a silicon substrate. Zero contact stiffness corresponds to no interaction between the indenter tip and specimen surface. For each individual indentation experiment, the first contact point [zoomed area, Fig. 2(a)] is accurately determined by the user during data analysis. For silicon, the contact stiffness is linear lyproportional to the displacement for indentation depths above 10 nm [Fig. 2(a)]. Deviations from this relationship at shallow depths can be explained by the non ideal geometry of the indenter tip. Hence, no reliable data for Young's modulus and hardness can be obtained within this depth range. For a 180 nm low-*k* film on a Si substrate, this depth range increases up to 15 nm due to the softness of the film [Fig. 2(b)].

2. Spatial extent of the elastic-deformation field

A commonly used procedure to reduce the elastic-deformation field during indentation is to increase the film thickness and compare the mechanical properties of different film thicknesses. However, as simple as this may seem, in many cases this is not a straightforward approach since it assumes similar mechanical properties and film stress states for all film thicknesses. In reality, both the mechanical properties and film stress state are very sensitive to the film fabrication process. In case of porous SiCOH low-*k* films, the mechanical properties of different thicknesses can only be compared when they contain similar film porosity, pore size distribution, and skeleton properties. Similar porosity for different film thicknesses can be achieved by optimizing the UV curing time. Thicker films need longer UV curing times, which results in a different strength of the skeleton or may even lead to hydrophilization of the film when UV overexposure takes place. Hydrophilization is detrimental during and after Cu/low-*k* integration since even a small amount of adsorbed water significantly increases the total *k*-value. This is especially important for porous materials, as they have a large surface area per unit volume where water could potentially be adsorbed. Even if the same skeleton properties can be achieved by fine tuning the UV-cure conditions, this cannot guarantee the same porosity or pore size distribution of the films. Hence, in order not to overcomplicate the main purpose of this work, we focused on 180 nm thick SiCOH low-*k* films. This thickness value is justified since it is close to thicknesses that are used in the present Cu/low-*k* integration scheme, but not too thin to be measured by nanoindentation (see Secs. III A 3 and III A 4). Another possible way to reduce the elastic-deformation field during indentation is by using shallow indentation depths. This can only result in accurate data if the indenter tip calibration is also accurate enough at these very low indentation depths. In Sec. III A 3 we will show that we can achieve a tip calibration sufficient enough to analyze film thicknesses as low as the ones studied in this work.

3. Indenter tip calibration

The key to measuring the mechanical properties of a material is knowing the contact area at each indentation depth. Therefore, a function relating the contact area (A) to the contact depth (h_c) is needed. For a perfect Berkovich tip this relationship would be given by $A(h_c)=24.56h_c^2$.[18,12] However

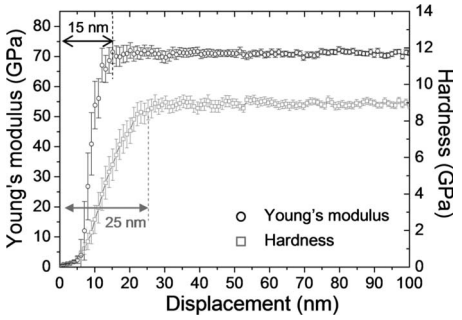

FIG. 3. Young's modulus and hardness depth profile of fused silica after performing the calibration of the indenter shape function using the CSM technique.

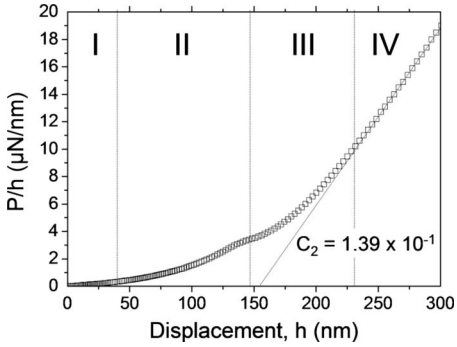

FIG. 4. P/h-vs-displacement curve for as-deposited material A1.

since indenters used in practical nanoindentation testing deviate from the ideal indenter shape, an expanded equation is used,

$$A(h_c) = 24.56h_c^2 + C_1h_c^1 + C_2h_c^{1/2} + C_3h_c^{1/4} + \cdots + C_8h_c^{1/128}, \quad (4)$$

where C_1–C_8 are calibration constants of the indenter tip that need to be determined by frequently performing independent indentations on a specimen that is mechanically isotropic and has a known Young's modulus and hardness that does not vary with indentation depth. Because of its ready availability and predictable mechanical properties, the most popular calibration material is fused silica (E=72 GPa, υ=0.17). Analysis routines are then used in reverse to deduce the tip-area function over a large range of indentation depths. In this work, the tip-area function was optimized to obtain reliable Young's modulus and hardness values for indentation depths up to 15 and 25 nm (Fig. 3), respectively. This is in agreement with the required penetration depths for reliable NI data [Fig. 2(b)].[23]

4. Determination of coating-only properties

In general, Young's modulus and hardness values measured by nanoindentation for thin films on substrates show severe substrate effects, thereby deviating from the "true" mechanical film properties. A common-held rule is that the penetration depth should be less than 10% of the film thickness in order to avoid severe substrate effects. However, this is certainly not a universal law but requires a good knowledge of the indentation-deformation behavior of the coating/substrate system, which is far more complicated than that of bulk materials. This is certainly true in the case of a soft film on a hard substrate, where significant pile-up effects may occur since the hard substrate will constrain the plastic deformation of the coating. Finding ways to separate substrate effects from the measured mechanical properties is, therefore, indispensable. Experimentally, in the case of a Berkovich indenter, the critical penetration depth may be experimentally determined by analyzing the load divided by the displacement (P/h) versus displacement (h) curves.[24,25] For most homogeneous elastoplastic materials, indentation loading curves obtained with self-similar indenter tips, such as Berkovich, conical, or pyramidal, are usually well described by[20,15]

$$P = Kh^2, \quad (5)$$

where K is a constant, depending on the properties of the material, such as Young's modulus, yield stress, and strain hardening.[26] For 180 nm thin SiCOH films on substrates, this relationship might deviate from its linear behavior depending on the relative stiffness of the film and substrate [Figs. 4 and 5(a)]. From the change in the P/h versus h relations, the indentation range containing the film properties without the severe effect of the substrate can be extracted. This is illustrated in Fig. 5(a), where a linear portion of the P/h curve is found for indentation depths up to 30 nm (stage I). Within this depth range, a plateau in Young's modulus and hardness is found, representing the film properties. The true meaning of this data is unclear since the effect of pore crushing during indentation of these porous low-k films is not well known. In this work, we will restrict to the comparison of mechanical film properties extracted from these observed plateaus. Future work includes a comparative study between NI experiments and finite-element modeling (FEM) to clarify the ef-

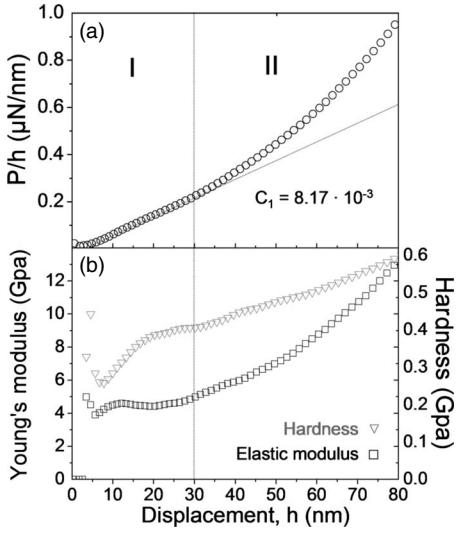

FIG. 5. (a) P/h-vs-displacement curve for as-deposited material A1 at low indentation depth; (b) corresponding Young's modulus and hardness.

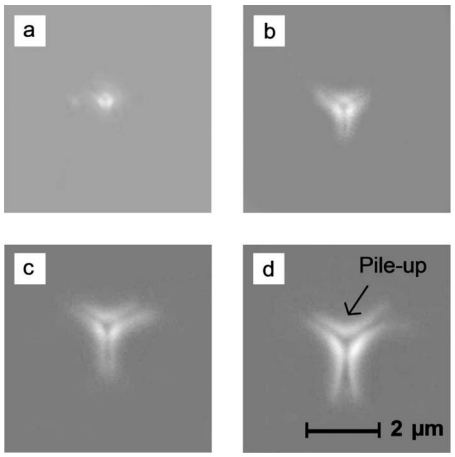

FIG. 6. Indentation deformation of a SiCOH-like low-*k* film on a Si substrate in (a) region II, (b) region III, and [(c) and (d)] region IV.

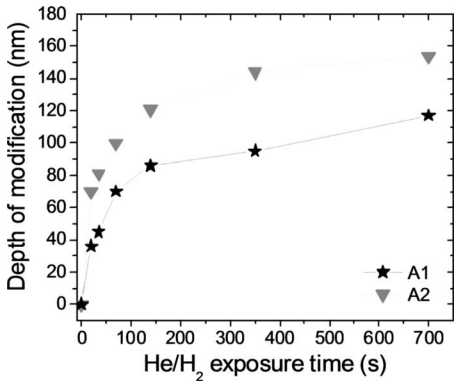

FIG. 7. Depth of modification as a function of He/H_2 plasma exposure time for films A1 and A2.

fects of pore crushing on the NI data. From stage II, the substrate starts to affect the measured results, where the slope of P/h deviates from the linear trend with higher values. A transition of the slope is found around 150 nm, corresponding to the indentation depth near the interface of the film and substrate. Such sudden change might be explained by de lamination or by film cracking. After this depth, the slope of the P/h curve increases (stage III, Fig. 4) until a second linear portion is reached (stage IV, Fig. 4). The rate of increase is faster than that found in stage II because in this stage, the indenter tip had been in contact with the substrate so that the measured mechanical properties in this stage are mainly coming from the hard Si substrate. Figure 6 show SEM images of material A1 at different indentation stages (stages II–IV). No indentation sites were found at stage I. Possible explanations for this might be that either the indentation size is too small at these shallow indentation depths or elastic recovery may have taken place while retracting the indenter tip. As the indenter approaches the interface with the substrate, significant pile-up areas were observed around the indentation imprints [Fig. 6(b)]. This pile-up is most likely related to the restricted deformation of the soft dielectric films on the hard silicon substrate. When the deformed area underneath the indenter tip reaches the interface between the film and the substrate, the material of the film will be pushed upward in order to release the energy that is introduced by the indentation event. Note that the mechanical thin-film properties (stage I) are found in the depth range where no pile-up effect was observed.

B. Mechanical properties of SiCOH low-*k* films upon He/H_2 exposure

Table I shows the physical properties of as-deposited low-*k* materials before and after UV cure. Both the hardness and Young's modulus are intimately linked to the variation in film porosity. The amount of porosity created in each film depends on the initial porogen concentration and the amount of porogen residues inside the films after UV curing.[7] Because for all films the same ratio of matrix and porogen precursors was used during deposition, the difference in porosity is mainly caused by the UV curing process. During this process, the porogen material is removed from the film, thereby introducing additional porosity to the films. Besides the removal of porogen material, UV curing also enhances the strength of the film skeleton. Using a broadband UV source (A2) clearly leaves less porogen residue as compared to a small band UV source (A1), as shown on the absorption spectra in Fig. 1. This agrees with the larger porosity and mean pore radii for film A2 (Table I). Note that the reported values actually reflect the mechanical properties of the top layer of the low-*k* films. It is clear that the initial mechanical properties of these films are very much determined by both the initial porogen content in the films, the remaining porogen residues and the strengthening of the film skeleton. Recently, it was found that all porogen residues can be removed by He/H_2-DSP independent of the wavelength of UV light that was used for curing and that no plasma damage has occurred in the low-*k* skeleton.[6,7] Hence, this approach offers an opportunity to study the effect of porogen residues on the mechanical properties. Figure 7 illustrates that the depth of modification for films A1 and A2 clearly increases with increasing He/H_2-DSP exposure time. In both cases the depth of modification tends to saturate at higher He/H_2-DSP exposure times suggesting that depth of porogen residue removal is limited by the diffusion of the H radicals into the low-*k* material. The observed difference in penetration depth between films A1 and A2 further illustrates that the penetration depth of H radicals is sensitive to the UV curing conditions (which defines the open porosity, pore size and pore size distribution of the films) and the recombination of H radicals on the pore walls. Figure 8 shows the relationship between Young's modulus and hardness for SiCOH low-*k* films that were exposed to He/H_2 plasma. During plasma exposure, no severe changes in total film thickness ($<1\%$) were found so that a relative comparison of the mechanical properties is still valid despite the rather small film thickness.[6] A clear decrease in the mechanical properties for increasing He/H_2 exposure times is found. Since no plasma damage was observed in the low-*k* skeleton upon He/H_2 treatment, this suggests that the observed decrease in the mechanical properties

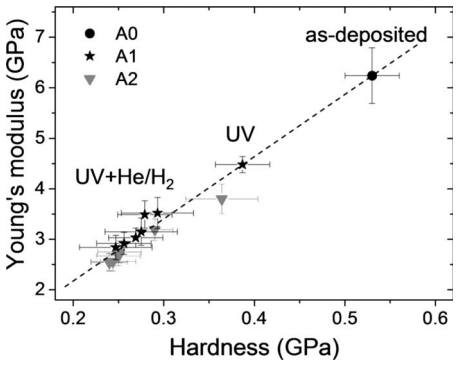

FIG. 8. Young's modulus and hardness for SiCOH low-*k* films that were exposed to He/H_2 plasma.

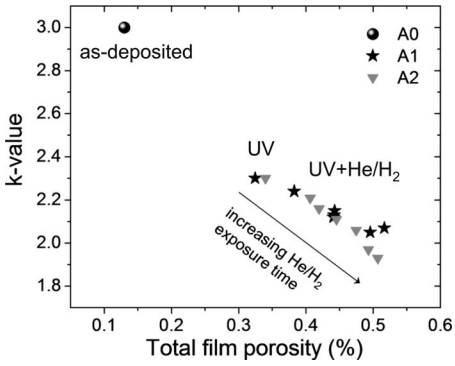

FIG. 10. Comparison between the total film porosity and the corresponding *k*-value of SiCOH low-*k* films before and after He/H_2 plasma exposure.

can be mainly attributed to the increased total film porosity caused by the removal of porogen residues inside the modified low-*k* film after He/H_2 treatment (Fig. 1). This reduction in mechanical properties corresponds to the materials ability to endure chemical mechanical polishing (CMP). It should be noted that CMP survivability is not a simple factor of Young's modulus, hardness, adhesion, or fracture toughness, but it is rather a combination of these properties that causes CMP-related failure.[27] Figure 9 shows the relationship between Young's modulus and porosity. Similar observations of influence of porogen residues on mechanical properties of porous methylsilsesquioxane films were reported by Maidenberg *et al.*[28] They found that by removing porogen residues using a short time UV/ozone exposure, a remarkable increase in fracture energy can be obtained from remnants of the porogen molecules. In literature, several models have been developed to describe the effect of porosity on mechanical properties. Some examples are cellular models for foam type solids,[29] percolation theory,[30] finite-element modeling,[31] or models based on fractal analysis.[32] However, it is not straightforward to quantitatively apply these models to the studied SiCOH low-*k* films. This is mainly because the mechanical properties of these films are not only defined by porosity and the pore size distribution, but also by the pore shape and the strength and structure of the skeleton. Figure 10 shows the relationship between the total film porosity and the corresponding *k*-value of the film. By increasing the total film porosity, the *k*-value of the studied films could be lowered to values as low as 2. The benefit of achieving such *k*-values is at the expense of reduced mechanical film properties (Fig. 8). Finding ways to further improve the film skeleton properties of porous low-*k* materials remains of great interest. Despite the clearly observed trends in Young's modulus and hardness for He/H_2 plasma-treated films, several questions still remain open for discussion.

- What is the effect of pore crushing and a collapsing film skeleton during indentation on the measured nanoindentation data?
- What is the actual contribution of the film skeleton to the measured values with nanoindentation and what is the role of porogen residues?
- How can the effect of porosity on the mechanical properties of PECVD SiCOH low-*k* films be described taking into account all the contributing factors?

Future work therefore includes FEM to validate the nanoindentation experiments presented in this work by investigating the influence of substrate properties. A comparative study between NI/FEM and surface acoustic wave spectroscopy (SAWS) may offer a way to clarify the contributions from the film skeleton and porogen residues to the global Young's modulus of the investigated films. Finally, also the He/H_2 plasma effect on the fracture toughness and interfacial adhesion will be studied.

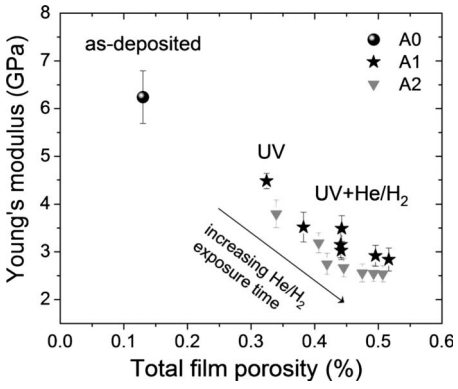

FIG. 9. Young's modulus vs total film porosity after He/H_2 plasma exposure.

IV. CONCLUSIONS

This work contained two parts. The first part focused on the main key factors that influenced the reliability of nanoindentation results of 180 nm PECVD low-*k* dielectric films. Good surface contact could be obtained for indentation depths above 15 nm. Hence, no reliable data could be obtained below this indentation depth. To improve the reliability of the nanoindentation data, the tip-area function was optimized to obtain reliable Young's modulus and hardness values at these shallow indentation depths. Furthermore, the effect of substrate on the film-only properties was analyzed by monitoring the change in P/h versus h curves. The linear range on the P/h curves, which defined the film properties,

was found at indentation depths below 17% of the low-*k* film thickness. In the second part of this work, the effect of He/H_2 downstream plasma at 280 °C on the mechanical properties of 180 nm PECVD low-*k* dielectric films was evaluated using nanoindentation and taking into account all the key factors that were encountered during the data analysis. Both the hardness and Young's modulus were intimately linked to the variation in film porosity. Observed trends in Young's modulus corresponded to trends in hardness. He/H_2 plasma caused a decrease in mechanical properties and a change in porosity, which was related to the removal of porogen residue. Moreover, the initial porogen content inside these films was proportional to the change in Young's modulus and porosity. This controlled increase in film porosity resulted in low-*k* films with reduced total *k*-value from 2.3 to 2.0. However, significant reduction in Young's modulus accompanied with increased porosity of the low-*k* films allows accounting for additional challenges during Cu/low-*k* integration. Future experiments involving FEM and SAWS are needed to clarify the contribution of porosity, porogen residues, and film skeleton on measured mechanical properties by nanoindentation.

[1]K. Maex, M. R. Baklanov, D. Shamiryan, F. Iacopi, S. H. Brongersma, and Z. S. Yanovitskaya, J. Appl. Phys. **93**, 8793 (2003).
[2]Y. L. Wang, C. Liu, S.-T. Chang, M.-S. Tsai, M.-S. Feng, and W.-T. Tseng, Thin Solid Films **308–309**, 550 (1997).
[3]H. Yano, Y. Matsui, G. Minamihaba, N. Kawahashi, and M. Hattori, Mater. Res. Soc. Symp. Proc. **671**, M2.4.1 (2001).
[4]C. L. Borst, V. Korthuis, G. B. Shinn, J. D. Luttmer, R. J. Gutmann, and W. N. Gill, Thin Solid Films **385**, 281 (2001).
[5]A. Urbanowicz, A. Humbert, G. Mannaert, Z. Tokei, and M. Baklanov, Solid State Phenom. **134**, 317 (2008).
[6]A. M. Urbanowicz *et al.*, Proceedings of the Advanced Metallization Conference, 2008 (unpublished), 593.
[7]A. Urbanowicz, K. Vanstreels, D. Shamiryan, S. De Gendt, and M. Baklanov, Electrochem. Solid-State Lett. **12**, H292 (2009).
[8]P. Marsik, A. Urbanowicz, P. Verdonck, K. Ferchichi, D. De Roest, L. Prager, and M. R. Baklanov, Mater. Res. Soc. Symp. Proc. **1079E**, N07 (2009).
[9]P. Marsik, P. Verdonck, D. Schneider, D. De Roest, S. Kaneko, and M. Baklanov, Phys. Status Solidi C **5**, 1253 (2008).
[10]I. L. Berry, Q. Han, C. Waldfried, O. Escorcia, and A. Becknell, SEMI Technical Symposium: Innovations in Semiconductor Manufacturing, 2004 (unpublished).
[11]M. Darnon *et al.*, J. Vac. Sci. Technol. B **26**, 1964 (2008).
[12]W. C. Oliver and G. M. Pharr, J. Mater. Res. **7**, 1564 (1992).
[13]X. Huang and A. A. Pelegri, J. Compos. Mater. **40**, 1393 (2006).
[14]T. Y. Tsui and G. M. Pharr, J. Mater. Res. **14**, 292 (1999).
[15]S. J. Bull, J. Phys. D: Appl. Phys. **38**, R393 (2005).
[16]F. Iacopi, Y. Travaly, and M. Van Hove, J. Mater. Res. **21**, 3161 (2006).
[17]J. B. Vella, A. A. Volinsky, I. S. Adhihetty, N. V. Edwards, and W. W. Gerberich, Mater. Res. Soc. Symp. Proc. **716**, 1 (2002).
[18]Y. Xiang, X. Chen, T. Y. Tsui, J.-I. Jang, and J. J. Vlassak, J. Mater. Res. **21**, 386 (2006).
[19]A. C. Fischer-Cripps, *Nanoindentation*, 2nd ed. (Springer, New York, 2004), pp. 69–110 and 132–143.
[20]A. Bolshakov and G. M. Pharr, J. Mater. Res. **13**, 1049 (1998).
[21]Y.-G. Jung and B. R. Lawn, J. Mater. Res. **19**, 3076 (2004).
[22]I. Manika and J. Maniks, J. Phys. D: Appl. Phys. **41**, 074010 (2008).
[23]M. F. Doerner and W. D. Nix, J. Mater. Res. **1**, 601 (1986).
[24]L. Shen, K. Zeng, Y. Wang, B. Narayanan, and R. Kumar, Microelectron. Eng. **70**, 115 (2003).
[25]I. N. Sneddon, Int. J. Eng. Sci. **3**, 47 (1965).
[26]P. L. Larsson, A. E. Giannakopoulos, E. Söderlund, D. J. Rowcliffe, and R. Vestergaard, Int. J. Solids Struct. **33**, 221 (1996).
[27]I. S. Adhihetty, J. B. Vella, A. A. Volinsky, C. Goldberg, and W. W. Gerberich, Proceedings of the Tenth International Congress on Fracture, ICF10, Honolulu, 2001 (unpublished).
[28]D. A. Maidenberg, W. Volksen, R. D. Miller, and R. H. Dauskardt, Nature Mater. **3**, 464 (2004).
[29]L. J. Gibson and M. F. Ashby, *Cellular Solids: Structure and Properties* (Pergamon Press, New York, 2000).
[30]J. Kováčik, J. Mater. Sci. Lett. **18**, 1007 (1999).
[31]A. P. Roberts and E. J. Garboczi, J. Am. Ceram. Soc. **83**, 3041 (2000).
[32]J. L. Plawsy, W. N. Gill, A. Jain, and S. Rogojevic, *Interlayer Dielectrics* (Elsevier, London, 2003), pp. 7–36.